Organic Electronics 46 (2017) 192–202

Contents lists available at ScienceDirect

Organic Electronics

journal homepage: www.elsevier.com/locate/orgel

Polymer solar cells based low bandgap A1-D-A2-D terpolymer based on fluorinated thiadiazoloquinoxaline and benzothiadiazole acceptors with energy loss less than 0.5 eV

M.L. Keshtov [a, **], S.A. Kuklin [a], A.R. Khokhlov [a], S.N. Osipov [a], N.A. Radychev [b], D.Y. Godovskiy [a], I.O. Konstantinov [a], F.C. Chen [c], E.N. Koukaras [d, e], Ganesh D. Sharma [f, *]

[a] Institute of Organoelement Compounds of the Russian Academy of Sciences, Vavilova St., 28, 119991, Moscow, Russian Federation
[b] Carl von Ossietzky University of Oldenburg, 26129, Oldenburg, Germany
[c] Department of Photonics, National Chiao Tung University, Hsinchu, Taiwan, 300, Taiwan, ROC
[d] Nanotechnology and Advanced Materials Laboratory, Department of Chemical Engineering, University of Patras, Patras, 26500 GR, Greece
[e] Molecular Engineering Laboratory, Department of Physics, University of Patras, Patras, 26500 GR, Greece
[f] Department of Physics, The LNM Institute for Information Technology (Deemed University), Jamdoli, Jaipur, India

ARTICLE INFO

Article history:
Received 21 February 2017
Received in revised form
7 April 2017
Accepted 13 April 2017
Available online 14 April 2017

Keywords:
Low bandgap terpolymer
Solvent additive and thermal annealing
Bulk heterojunction solar cells
Power conversion efficiency

ABSTRACT

We synthesized an ultra low bandgap terpolymer denoted as P containing fluorinated-fluorene attached thiadiazoloquinoxaline and benzothiadiazole acceptors and thiophene as donor in its backbone and investigated its optical and electrochemical properties. This terpolymer is used for as donor along with $PC_{71}BM$ as electron acceptor in solution processed polymer solar cells (PSCs). The **P** showed a shows strong absorption band from 650 nm to 1100 nm with an optical bandgap of 1.12 eV and highest occupied molecular orbital (HOMO) and lowest unoccupied molecular orbital (LUMO) energy levels of −5.25 eV and −3.87 eV, respectively. After the optimization of **P** to $PC_{71}BM$ weight ratio, the optimized weight ratio 1:2 in chlorobenzene (CB) solution, the PSC showed overall power conversion efficiency of 4.10% (J_{sc} of 10.96 mA/cm^2, V_{oc} of 0.68 V and FF of 0.55). After the solvent additive (3 v% DIO) followed by subsequent thermal annealing (SA-TA) the PCE has been increased up to 7.54% with J_{sc} of 16.12 mA/cm^2, V_{oc} of 0.65 V and FF of 0.72. The increase in the PCE is related with the enhancement in the both J_{sc} and FF, attributed optimized nanoscale morphology of the active layer for both efficient exciton dissociation and charge transport towards the electrodes and balanced charge transport in the device, induced by the TSA treatment of the active layer. This is the highest PCE of PSCs with an energy loss about 0.47 eV with the low bandgap of 1.12 eV.

1. Introduction

Polymer solar cells (PSCs) based on bulk heterojunction (BHJ) active layer are the promising candidates to convert the solar energy into electrical energy, due to their low cost, light weight, large scale production from the solution processing and mechanical flexibility which impart the green energy technology at low cost [1–8]. In a BHJ PSC whose active layer is composed by donor (conjugated polymers and small molecules) and acceptor (fullerene derivatives and non-fullerene small molecules) phases, the nanoscale morphology of the active layer provides important pathways for charge generations, carrier transports, and collections at electrodes, which would significantly influence the photovoltaic performance [9–11]. Through constant improvement in organic materials and device structure, power conversion efficiencies (PCEs) of PSCs has been achieved more than 10% at lab scale level and 7% at module level, respectively, after the constant improvement in the optical and electrochemical properties of organic materials and device structure, consequence the potential of PSCs for applications in solar energy conversion [12–19]. The PCE of the PSCs is highly influenced by the light harvesting ability of the electron donating polymer. Therefore, efficient harvesting of solar energy requires the development of new polymers with high absorption coefficient and extended absorption spectra in order to

* Corresponding author.
** Corresponding author.
E-mail address: sharmagd_in@yahoo.com (G.D. Sharma).

http://dx.doi.org/10.1016/j.orgel.2017.04.015
1566-1199/

enable photocurrent generation from longer wavelength region of solar spectrum. This in turn will require low energy bandgap polymers that absorb at near infrared (NIR) wavelengths. While the size of the energy gap has great importance in the design of these materials, it is important to tailor the energy difference between the HOMO of the polymer donor and the LUMO of the fullerene acceptor in the BHJ active layer. The development of low band gap conjugated copolymers with donor-acceptor (D-A) alternating structure have concerned great deal of attention because their electronic properties can be easily tuned by proper combination of D and A units [20–22]. Moreover, the energy level control of the D-A type polymers facilitates the intramolecular charge transfer (ICT) transition, which results in reduced band gaps and thus the absorption ranges can be extended to longer wavelengths [23–26]. In order to cover a broader spectrum of solar irradiation, development of semiconducting polymers with high absorption coefficients extended absorption in near infrared region and efficient harvesting of solar energy is required. This in turns require low energy gap polymers that absorb at near IR wavelengths. Although the size of the energy bandgap has great importance in the design of these materials, it is also important to tailor the energy difference between the HOMO of the polymer donor and LUMO of the fullerene acceptor in the BHJ, since this difference is directly related to the V_{oc} of resulted PSC. Moreover, for high J_{sc}, the difference in LUMO offset between the donor and acceptor must by higher than that of binding energy of the exciton, for efficient exciton dissociation [27]. By selecting the proper donor (electron rich) and acceptor (electron deficient), units, the optical and electrochemical properties of resultant copolymer can be tailored [28,29]. In general stronger electron donors and stronger acceptors reduce the optical bandgap. Moreover, introducing a third monomer into the D-A polymer backbone (i.e. A1-D-A2-D or A-D1-A-D2-A), the optical and electrochemical and charge carrier mobility can be easily tailored, leading to the improvement in PCE of resulting PSCs via synergy between the three monomers [30–40].

In PSCs, the large energy loss (E_{loss}) (0.7–1.0 eV) is one of crucial issues for their low PCEs. The large Eloss is associated with the larger driving force for excitons dissociation and large non-radiative recombination [41]. Therefore, it is needed that the energy loss should be minimized to increase simultaneously both J_{sc} and V_{oc} and thereby improving the overall PCE of the PSCs, by designing low polymeric donor materials with low bandgap and suitable energy levels.

Thiadiazoloquinoxaline (TDQ) is a promising building block for the synthesis of ultra low bandgap D-A copolymers due to its strong electron withdrawing properties due to four imino groups in TDQ units. It is reported that the fluorination on the polymer backbone has shown immense advantages such as (i) lowering the HOMO energy level of conjugated polymer thereby increasing the V_{oc} of the resulting PSCs [42], (ii) increasing the dipole moment between the ground state and excited state of the polymer which can suppress the charge recombination, resulting the improvement in the J_{sc} and FF [43,44], and (iii) enhancing the inter/intramolecular interaction of the polymers, leading to high charge carrier mobility [45]. Therefore, fluorination of the polymer backbone has become one of the strategies in tailoring the molecular structure to achieve the high performance PSCs [46–49]. Moreover, the incorporation of different numbers of fluorine atoms would definitely change the structural symmetry of the repeat units, leading to the regioregular polymer structure, which is crucial for photovoltaic properties [50–52]. We have synthesized a A1-D-A2-D terpolymer denoted as **P** that contain two different A1 bis-(9,9-didodecyl-7,9-fluoro-fluoren-2-yl)-[1,2,5]thiadiazolo[3,4-g]quinoxaline (ffFlTDQ$_x$) and A2 benzothiadiazole (BT) acceptor groups and thiophene donor in repeating unit. The newly synthesized terpolymer exhibits a broad absorption profile ranging from 350 nm to 1100 nm with optical bandgap of 1.12 eV and demonstrated good solubility in most of the common organic solvents due to alkyl lateral substituents. We have employed **P** as electron donor along with the $PC_{71}BM$ as electron acceptor for solution processed BHJ PSCs. After the optimization of P to $PC_{71}BM$ weight ratio and combined solvent additive followed by thermal annealing (SA-TA), the PSC showed overall PCE of 7.54% with low energy loss of 0.47 eV.

2. Experimental

2.1. Synthesis of terpolymer *P*

Monomers **M1** (0.7098 g, 0.5 mmol), **M2** (0.4122, 0.5 mmol) and $Pd(PPh_3)_4$ (0.027 g, 0.023 mmol) were dissolved in 15 ml of dry toluene. Reaction mixture was heated at 110 °C for 48 h in argon atmosphere. After cooling the product was precipitated with methanol (200 ml) and filtered. The raw polymer was dissolved in small volume of chloroform and precipitated with methanol again and then it was additionally purified by means of sequential extractions with methanol, hexane and chloroform. Chloroform fraction was concentrated and precipitated with methanol. The terpolymer **P** was filtered and dried in vacuum. The yield is 78%.

2.2. Device fabrication and characterization

The PSCs were fabricated with a conventional structure ITO/PEDOT:PSS/**P**:$PC_{71}BM$/PFN/Al. First of all the indium tin oxide (ITO) coated glass substrates were cleaned, inside ultrasonicated bath, beginning with acetone, followed by deionized water and isopropanol and then dried in an oven at 40 °C for 2 h. After drying a 40 nm thin PEDOT:PSS (Clevios P AI4083) anode buffer layer was spin-cast onto the ITO substrate and then dried by baking in a vacuum oven at 100 °C for overnight. The active layers i.e. **P**:$PC_{71}BM$ in different weight ratios were deposited onto the top of PEDOT:PSS layer, by casting from chlorobenzene solution and then dried in ambient conditions. For the SA-TA treatment the optimized **P**:$PC_{71}BM$ (1:2) active layer was spin coated with DIO (3 v%)/CB solution and then thermally annealed at 120 °C for 30 s. The PFN solution in methanol was spin-coated on the top of the obtained active layer to form a thin interlayer of 5 nm. Finally, a thin layer of aluminium (Al) layer with thickness of 100 nm was thermally evaporated with a shadow mask at a base pressure of ~10^{-6} Torr. The overlapping area between the cathode and anode defined a pixel size of 16 mm^2. The fabrication of the devices was done at ambient conditions.

A Keithley Source Meter was used to measure the current-voltage (J-V) characteristics of the solar cells in ambient conditions and under AM1.5 G (100 mW/cm^2) provided by a solar simulator. The incident photon-to-current efficiency (IPCE) of the devices was measured by illuminating the devices through the light source and a monochromator and the resulting current was measured using a Keithley electrometer under short-circuit conditions.

In order to measure the hole and electron mobilities in the active layers, we have fabricated hole and electron only devices i.e. ITO/PEDOT:PSS/active layer/Au and ITO/Al/active layer/Al, respectively and then measured the current −voltage characteristics under dark.

3. Results and discussion

3.1. Synthesis and characterization of *P*

Synthetic route for the synthesis of terpolymer **P** is presented on

Scheme 1 along with the chemical structure of non-fluorinated terpolymer P1. In order to prepare novel narrow bandgap polymers, we initially had prepared aromatic di-bromide **M1** [53] and **M2** [54] in accordance to literature methods. Interaction of equimolar amounts of fluorinated aromatic di-bromide **M1** and **M2** in refluxing toluene for 48 h in the presence of $Pd(PPh_3)_4$ under Stille reaction conditions gives new alternating narrow bandgap terpolymer **P** (Scheme 1). Reaction was conducted in homogeneous conditions and allowed to obtain the polymers with reasonable high yields and moderate molecular weights; it allowed preparing sufficiently durable polymeric films for photovoltaic investigations. The polymers were purified by double precipitation of their chloroform solutions with methanol and sequential extraction of solids with methanol, hexane and chloroform using Sohxlett apparatus. Chloroform fractions were concentrated to minimal volume and precipitated with methanol, solid precipitates were filtered and dried in vacuum at 80 °C for 24 h. Yield of the **P** was 78% and has good solubility in chlorinated solvents such as chloroform, chlorobenzene or o-dichlorobenzene. Composition and structure of **P** were confirmed by ^{1}H NMR spectroscopy (Fig. S1, supplementary information). Molecular weights of the polymers were elucidated with gel-permeation chromatography (GPC) with polystyrene as standard. Number-averaged (M_n) and weight-averaged (M_w) molecular weights and polydispersity (M_w/M_n) of copolymer **P** were estimated to be 9700 kDa, 23870 kDa and 2.46, respectively.

Thermal properties of copolymer play an important role in BHJ PSCs. Thermal property of the **P** was studied with thermogravimetric analysis (TGA) as shown in Fig. S2 (supplementary information). As shown in Fig. S2 that 5% weight loss temperature of copolymer is high enough 368 °C, indicating that the terpolymer **P** is quite stable for applications in photovoltaic and other optoelectronic devices.

3.2. Optical properties and electrochemical properties

Optical properties of terpolymer **P** were investigated by means of UV spectroscopy and shown in Fig. 1 and results were summarized in Table 1. Absorption maxima of **P** in solution showed dual absorption bands in shorter wavelength (350–650 with peak at 390 nm) and longer wavelength region (650–1000 nm with a peak at 924 nm) can be assigned π-π* transitions in terpolymer

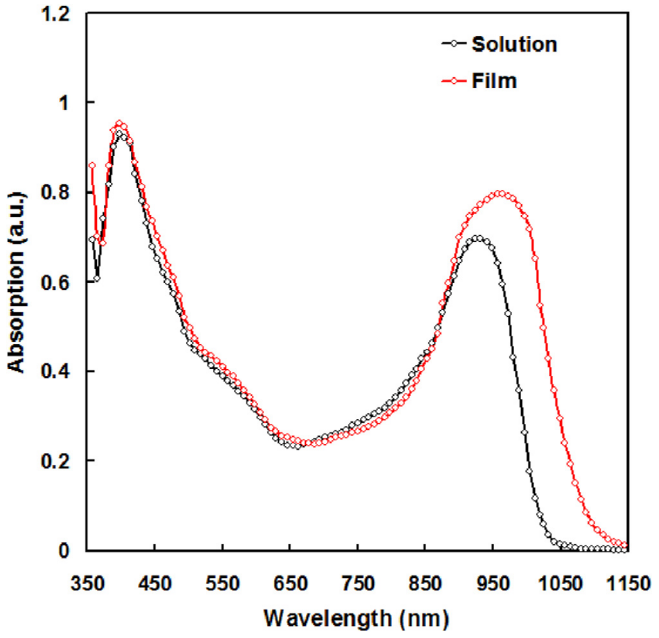

Fig. 1. Optical absorption spectra of **P** in chloroform solution and thin film cast from CB.

Table 1
Optical and electrochemical properties of terpolymer **P**.

Polymer	λ^{soln}_{max} (nm)	λ^{film}_{max} (nm)	E_g^{opt} [a] (eV)	E^{ec}_{HOMO} (eV)	E^{ec}_{LUMO} (eV)	E_g^{ec} (eV)
P	390, 924	390, 958	1.12	−5.25	−3.83	1.42

[a] Estimated from the absorption band onset of thin film, $E_g^{opt}=1240/\lambda^{film}_{onset}$.

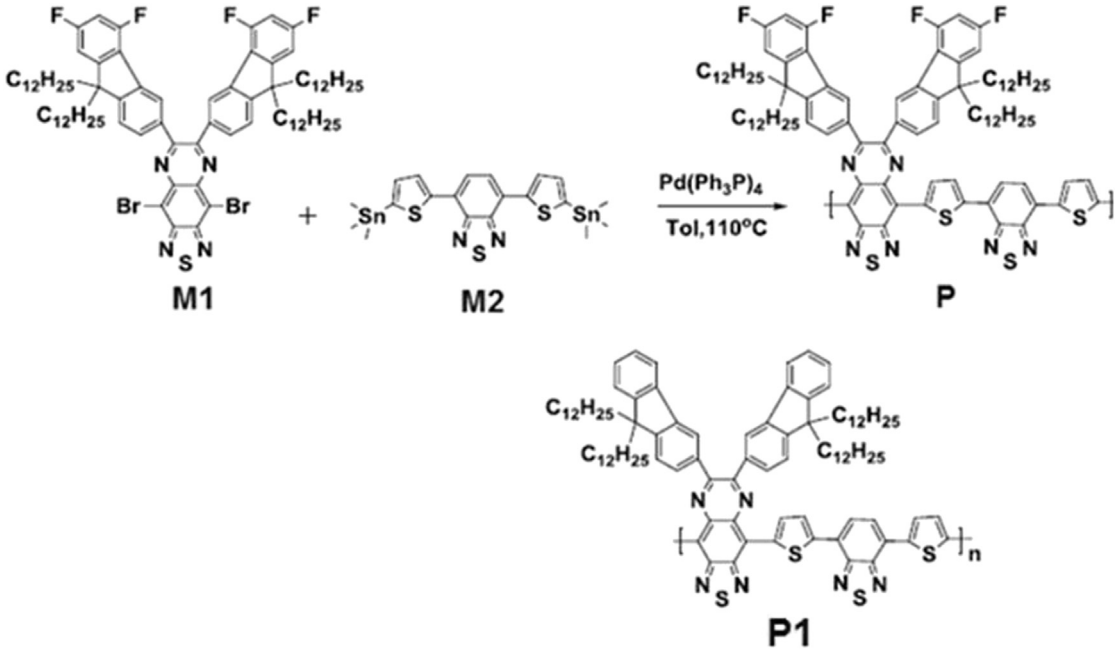

Scheme 1. Synthetic routes of terpolymer **P** and chemical structure of non-fluorinated counterpart P1.

backbone and intramolecular charge transfer (ICT) between the donor and acceptor units present in the terpolymer, respectively [55]. Absorption spectrum in thin film of the **P** exhibited broader bands and bathochromic shift compared with the absorption spectrum in solutions and probably caused by intermolecular interactions between the terpolymer chains, aggregation of macromolecules and more structured and improved packaging of polymeric molecules of **P** in solid film compared to that in solution. Optical bandgap values (E_g^{opt}) of **P** was estimated from the absorption onsets and is of 1.12 eV. The broad ranges of absorption (350–1100 nm) and narrow bandgap of the terpolymers favor for their application as electron donors in PSCs.

Electrochemical properties of terpolymers **P** were studied by means of cyclic voltammetry (Fig. 2) and the results are listed in Table 1. Onsets of oxidation (E_{ox}^{on}) and reduction (E_{red}^{on}) potentials of **P** were determined from the cyclic voltammograms and are of 0.85 V and −0.53 V, respectively. The HOMO and LUMO energy levels and electrochemical bandgap values (E_g^{ec}) of **P** were estimated by following equations:

$$\text{LUMO} = -e(E_{red}^{on} + 4.4)\ (\text{eV})$$

$$\text{HOMO} = -e(E_{ox}^{on} + 4.4)\ (\text{eV})$$

$$E_g^{ec} = e(E_{ox}^{on} - E_{red}^{on})\ (\text{eV})$$

The values of HOMO and LUMO energy levels of **P** were estimated from the onsets of oxidation and reduction potentials, respectively and are −5.25 eV and −3.87 eV, respectively and corresponding electrochemical bandgap is 1.42 eV. The HOMO level of P is deeper than its non-fluorinated counterpart terpolymer P1 (−5.08 eV) [56].

3.3. Theoretical calculations

We have theoretically studied the terpolymer **P** and its non-fluorinated counterpart P1 structures within the framework of density functional theory (DFT) and time-dependent density functional theory (TD-DFT). For both DFT and TD-DFT computations we employed the gradient corrected functional PBE [57], the hybrid functional B3LYP [58], and the meta-hybrid functional M06 [59]. Technical details on the computations are provided in the Supporting Information.

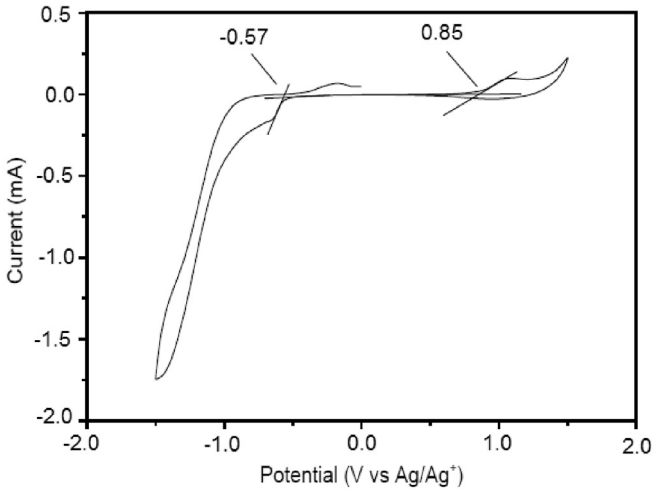

Fig. 2. Cyclic voltammograms of film **P** cast on a platinum electrode in 0.1 mol L^{-1} Bu_4NClO_4/CH_3CN at a scan rate of 50 mV s^{-1}.

The main body of the structure, that consists of thiadiazoloquinoxaline (**TDAQ**) and dithiophene-benzothiadiazole (**TBTDA**) moieties, is highly planar with dihedral angles between these moieties, as well as the thiophenes, in the range of ~1°–5°, depending on the functional and the presence of solvent. The **TDAQ** moieties of P1 and **P** have attached didodecyl-fluorene and didodecyl-tetrafluoro-fluorene groups, respectively. These groups are out of plane and form dihedrals angles 38°–49° and 35°–45° with the plane of the main body, for **P1** and **P** respectively. We have calculated the HOMO and LUMO energy levels and the optical gaps, defined here as the energetically lowest allowed vertical electronic excitation, employing the PBE, M06, and B3LYP functionals. In addition to the frontier orbitals' energy levels, we also provide the optical gap the main contributions to the first excitation as well as the wavelength of the first excitation and of the excitations with the largest oscillator strengths and complied in Table 2.

The effect of fluorination of the fluorene groups is a negligible lowering of both the HOMO and the LUMO levels, and by nearly the same amount, leaving the computed HOMO–LUMO (HL) gap unchanged. The ultraviolet/visual absorbance profiles remain almost the same with a minor exception at the intermediate wavelength region where there is a slightly broader absorbance in the case of the fluorinated structure **P**. Any improvement in the photovoltaic performance of the actual device is thus attributed to more efficient stacking between the fluorinated polymers and not to changes in the absorbance profiles of the individual molecular structures (polymers). Similar effects have also been identified by Deng et al. [60] in small molecules, that reported increase in PCE with increasing fluorination of end-capped groups. This was found to be a direct result of denser and more ordered π–π stacking for the fluorinated species.

The energy gaps calculated using the hybrid B3LYP functional is underestimated compared to value using the meta-hybrid M06 functional. For the HOMO–LUMO (HL) gap the values computed using B3LYP are lower by ~0.35 eV and for the optical gaps by ~0.1 eV. In Table 1 we also provide the character of the first allowed excitations only for contributions larger than 4%. The first excitation, as calculated by each of the functional clearly exhibits a single-configuration character. In Fig. 3 we have plotted the isosurfaces of the HOMO and LUMO of P1 and **P**. The HOMO extends over the main body with a higher localization over the **TBTDA** moiety. The LUMO is more localized over the **TDAQ** moieties. This is also shown by the partial density of states that we provide in the Supporting Information (Supporting Information Fig. SI-1). The first notable effect of fluorination on the computed partial density of states is on the contribution of fluorene to states at −7.2 eV that slightly deepens to −7.7 eV. These are energetically deep levels that correspond to HOMO–5 and HOMO–6 for P1, and are not involved in any moderate to strong excitations (i.e., no less than 10% of maximum noted oscillator strength) of the UV/Visible spectra. For **P** these states correspond to HOMO–7 down to HOMO–9 that we find contribute moderately to energetically high excitations with wavelengths in the region of ~335 nm. Upon fluorination, a significant decrease is also noted in the contribution of the fluorene group to even deeper states at −10 eV. The computed UV/Visual absorbance spectra the **P1** and **P** structures calculated at the TD-DFT/M06 and B3LYP level of theory are given in the Supporting Information (see Figs. SI-2, SI-3), both accounting for solvent effects for chlorobenzene and in gas phase. The spectra obtained from the two functionals are found to be in excellent agreement on the form and range, and are found to exhibit four peaks. The peaks are centered about 340 nm, 455 nm, 520 nm and 727 nm and are of comparable intensity. The positions of the peaks computed using the B3LYP functional are slightly redshifted, by ~16 nm in the short wavelength region, and by ~40 nm in the long wavelength region.

Table 2
Calculated properties of P1 and **P**. Specifically, HOMO and LUMO energies (eV), HOMO–LUMO gap (eV), *HL*, Optical gap (eV), *OG*, with corresponding oscillator strengths, *f*, the wavelengths of the first excitation and excitations with the largest oscillator strengths, the main contributions to the first excited state, and the dipole moment (D), μ.

	HOMO (eV)	LUMO (eV)	HL (eV)	OG (eV)	$\lambda_{1st/max}$ (nm)	*f*	Main Contributions	μ (D)
P1								
PBE	−4.74	−3.80	0.94	1.32	937	0.30	H→L (90%); H→L+2 (6%)	3.95
	−4.87[a]	−3.91[a]	0.96[a]	1.27[a]	976[a]	0.42[a]	H→L (94%)	5.13[a]
B3LYP	−5.25	−3.38	1.88	1.67	743/573/456/376/349	0.48	H→L (99%)	3.47
	−5.39[a]	−3.47[a]	1.91[a]	1.62[a]	765/574/467/369/348[a]	0.64[a]	H→L (99%)	4.30[a]
M06	−5.55	−3.31	2.24	1.75	708/539/431/357/333	0.46	H→L (98%)	3.55
	−5.69[a]	−3.42[a]	2.27[a]	1.71[a]	726/542/443/354/334[a]	0.64[a]	H→L (98%)	4.57[a]
P								
PBE	−4.77	−3.83	0.94	1.32	939	0.30	H→L (90%); H→L+2 (6%)	2.78
	−4.87[a]	−3.91[a]	0.96[a]	1.27[a]	977[a]	0.43[a]	H→L (94%)	3.98[a]
B3LYP	−5.29	−3.41	1.87	1.67	744/572/449/379/350	0.48	H→L (99%)	2.00
	−5.39[a]	−3.48[a]	1.91[a]	1.62[a]	767/574/462/372/351[a]	0.64[a]	H→L (99%)	2.88[a]
M06	−5.59	−3.35	2.24	1.75	709/539/433/362/337	0.47	H→L (98%)	1.98
	−5.70[a]	−3.43[a]	2.27[a]	1.71[a]	726/541/497/444/333[a]	0.63[a]	H→L (98%)	3.00[a]

[a] Values when solvent effects are taken into account for chlorobenzene.

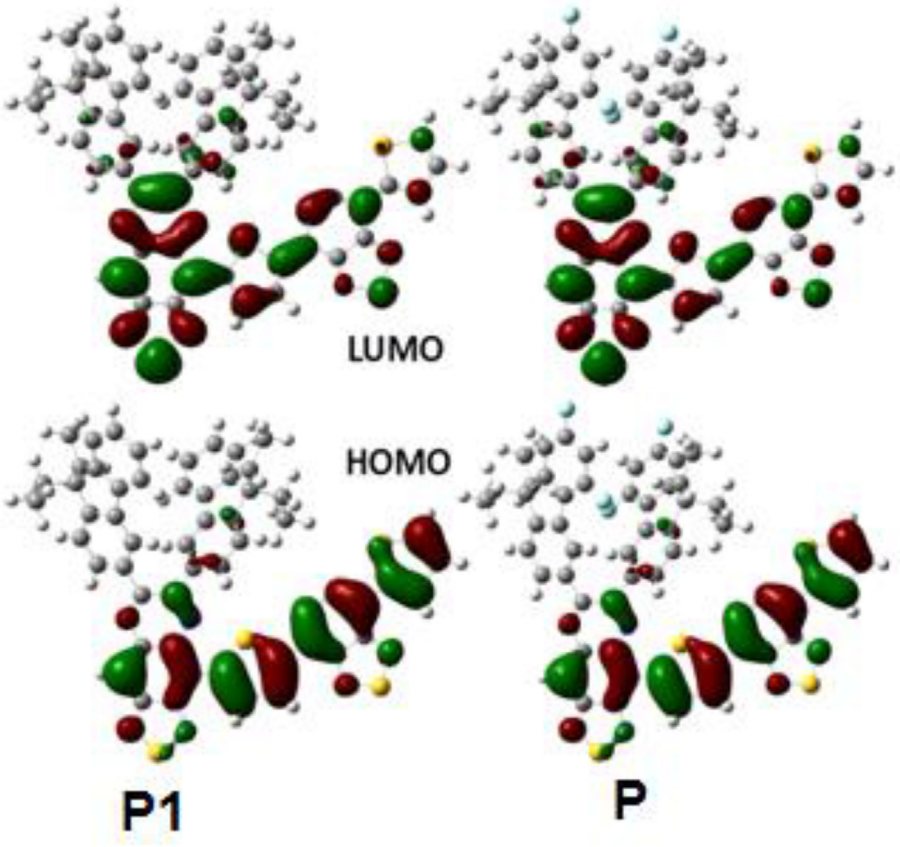

Fig. 3. Frontier orbitals of **P1** and **P**. (top) LUMO, and (bottom) HOMO. (isovalue = 0.02).

3.4. Photovoltaic properties

In a BHJ PSC, the relative amount of the donor and acceptor materials employed in a blend active layer is a crucial factor for overall PCE, since there should be a balance between absorbance (the photons are mainly absorbed by donor material) and charge carrier (holes and electrons in donor and acceptor phases, respectively) transport in the active layer. When the acceptor content is too low, the electron transporting ability will be limited, while when the acceptor content is high, the absorbance and hole transport ability in the active layer will be decreased. The donors to acceptor weight ratio significantly affect the overall PCE of the device and mainly attributed to the J_{sc} and FF. The BHJ active layers with the mixture of P and $PC_{71}BM$ blended in CB in different weight ratios (1:1, 1:1.5, 1:2, and 1:2.5) were prepared and their photovoltaic performances using the architecture ITO coated glass/PEDOT:PSS/active layer/PFN/Al were investigated and the photovoltaic parameters of PSCs with different P to $PC_{71}BM$ weight ratios are complied in Table S1 (supplementary information). The optimum device performance was found for the 1:2 ratio processed with CB. The PSCs were fabricated by spin coating the active layer processed with 3 v % DIO/CB, (solvent additive) solution and followed by thermal annealing at 110 °C for 10 min i.e. combined solvent additive and thermal annealing (SA-TA) to improve the

active layer morphology. The current −voltage (J-V) characteristics under illumination (AM1.5, 100 mW/cm^2) are shown in Fig. 4a and photovoltaic parameters are shown in Table 3. Under the optimized conditions, the PSC based on active layer (1:2) processed with CB showed the PCE of 4.10% with J_{sc} of 10.96 mA/cm^2, V_{oc} of 0.68 V and FF of 0.55 which is higher than that for the device based on non-fluorinated counterpart [56].

The PCE of the PSC based on active layer **P**:$PC_{71}BM$ cast from CB is low may be due to the poor nanoscale morphology of the active layer. Since organic semiconductors (both conjugated polymers and small molecules) have short exciton diffusion lengths and large exciton binding energies due to their low dielectric constant. When these materials used as donor along with acceptor organic semiconductors in a BHJ architecture, ideal self assembled nanoscale morphology with enlarged interfacial area with a bicontinuous interpenetrating network of electron donors (polymers) and acceptor (fullerene derivatives) is required to improve the photo-induced charge transfer, exciton dissociation and charge collection [61,62]. In order to further improve the PCE of the PSC, the optimized layers were also optimized with solvent additive (SA) followed by thermal annealing (SA-TA). The processing additive, 1,8-diiodooctane (DIO, 3 v%) was added into the optimized mixture solution of **P**:$PC_{71}BM$ (1:2) in CB prior to spin coating and then annealed at 120 °C for 10 min. The J-V characteristics of the best device are shown in Fig. 4a and photovoltaic parameters were complied in Table 1. After the treatment of TSA, the PCE of the PSC have been improved up to 7.54% with Jsc of 16.12 mA/cm^2, Voc of 0.65 V and FF of 0.72. The IPCE spectra of the devices (Fig. 4b) are closely resemble with the absorption spectra of corresponding active layers (Fig. 5) and had a response in the wavelength range of 350–1100 nm. The highest IPCE values of the devices based on as cast and TSA treated active layers are 55% and 72%, respectively.

Although the P exhibits deeper HOMO level than its non-fluorinated counterpart, but the observed Voc of the PSC is lower than that for PSC based on non-fluorinated terpolymer. It should be noted that in our case with the incorporation of fluorine atoms increase of the value of Jsc of the corresponding device. This could be due to the introduction of fluorine into polymer chain and increases of intermolecular interaction of in the backbone of polymer due to strong induced C–F bond that leads to high charge mobility and transport. Furthermore strong F···H/F···S interaction and well-resolved fluoropolymers fibril structure can make significant contribution to active level morphology, more planar conjugated backbone and improved π-π stacking and to suppress charge recombination.

The absorption spectra of the SA-TA processed active layer

Table 3
Photovoltaic parameters of the PSC based on **P**:$PC_{71}BM$ processed under different conditions.

Active layer	J_{sc} (mA/cm^2)	V_{oc} (V)	FF	PCE (%)
As cast	10.96	0.68	0.55	4.10 (3.98)[a]
SA-TA	16.12	0.65	0.72	7.54 (7.42)[a]

[a] Average of 10 devices.

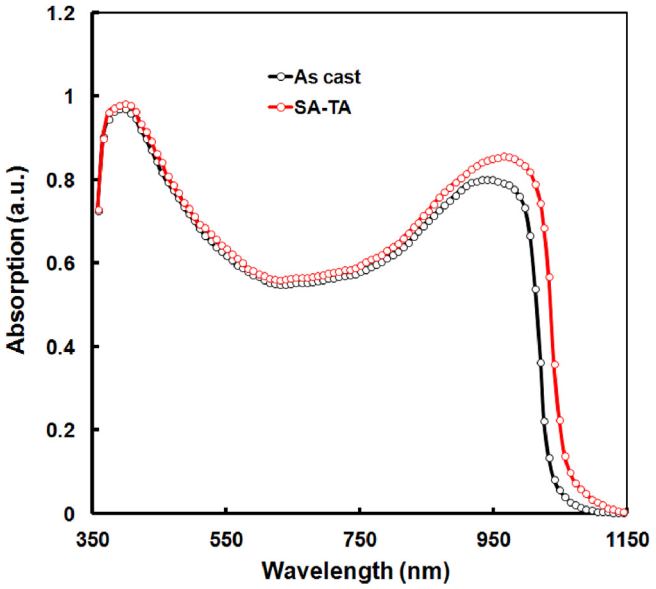

Fig. 5. Normalized absorption spectra of as cast and SA-TA treated **P**:$PC_{71}BM$ active layers.

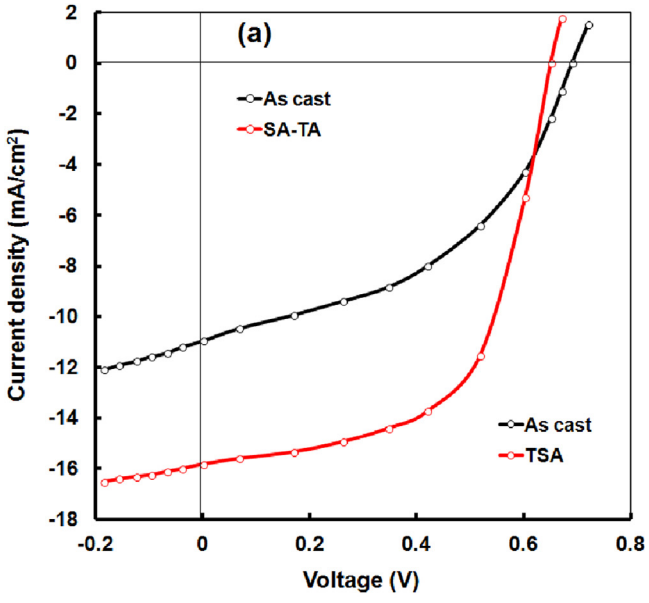

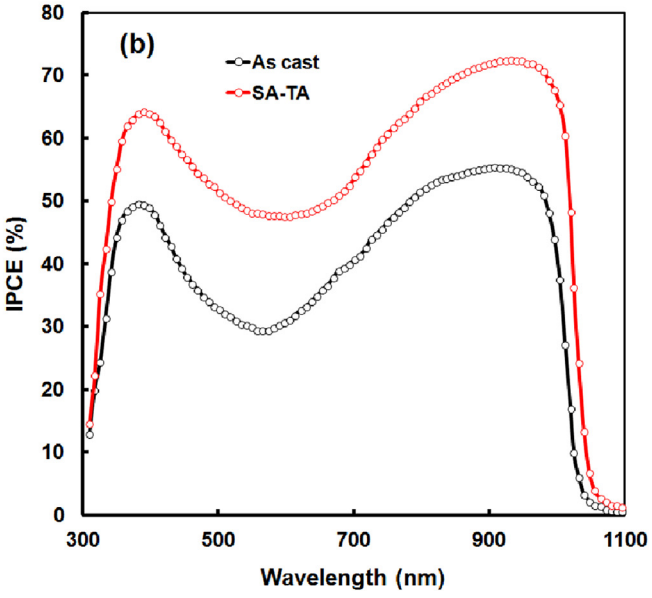

Fig. 4. (a) Current–voltage (J–V) characteristics and (b) IPCE spectra of **P**:$PC_{71}BM$ (1:2 w/w) devices processed with as cast from CB and SA-TA treatment.

exhibit higher absorption coefficient and redshifted as compared to that for CB cast counterpart (as shown in Fig. 5). The absorption efficiency (η_A) of CB cast and TSA processed active layer with same thickness is determined by the following expression [63,64]:

$$\eta_A = \frac{\int \left(1 - 10^{-\alpha d}\right) S(\lambda) d\lambda}{\int S(\lambda) d\lambda}$$

where S(λ) is the photon flux, i.e. number of photon at wavelength λ in AM1.5 G solar spectrum, α is the absorption coefficient and d is the thickness of the active layer. The values of ηA are estimated to be 34.45% and 36.23% for as cast and SA-TA processed **P**:$PC_{71}BM$ active layers, respectively. Therefore, the number of photo-generated excitons may be higher for TSA processed **P**:$PC_{71}BM$ than CB cast counterpart, attributed to the large overlap between the solar spectrum of SA-TA processed active layer. The J_{sc} values estimated from the integration of IPCE spectra are 10.84 mA/cm^2 and 16.01 mA/cm^2 for as cast and SA-TA treated active layers, respectively and are very close to the values observed in the J-V characteristics of the devices under illumination.

In order to investigate the charge collection properties, the hole and electron mobilities were measured for as cast and SA-TA treated active layers from the dark current −voltage characteristics (J-V) of the hole only (ITO/PEDOT:PSS/active layer/Au) and electron only (ITO/Al/active layer/Al) devices, respectively. The J-V characteristics of hole and electron only devices are presented in Fig. 6a and b, respectively and fitted with Mott-Gurney law:

$$J = \frac{9}{8} \varepsilon \varepsilon_o \mu \left(\frac{V^2}{L^3}\right)$$

where J is current density, ε is the relative dielectric constant of active layer, ε_o is the permittivity of free space, μ is the charge carrier mobility, L is the thickness of active layer and V is the effective applied voltage on the active layer. Fitting J-V characteristics with space charge limited current model (SCLC) [65], the hole mobilities in the as cast and SA-TA treated active layers are 3.36 × 10^{-5} cm^2/V and 1.45 × 10^{-4} cm^2/V respectively, while the values of electron mobility are 2.54 × 10^{-4} cm^2/V and 2.63 × 10^{-4} cm^2/V, respectively for as cast and SA-TA treated active layers. The hole mobility for SA-TA treated active layer is higher indicating more balanced charge transport in corresponding PSC, leading to improved J_{sc}, FF and PCE.

In order to get information about the influence of SA-TA on the charge recombination kinetics, the variation of J_{sc} with light intensity was measured (Fig. 7) which allows determination of important factors that control the FF owing to strong relation between the charge recombination and exciton quenching in the BHJ active layers [66]. In general, variation of Jsc with incident illumination intensity (P_{in}) showed a power law dependence as $J_{sc} \propto (P_{in})^{\gamma}$, where γ is exponent, which is close to 1, if the bimolecular recombination between the hole and electron is negligible [67]. As can be seen from Fig. 7, the values γ are 0.95 and 0.89 for the devices based on SA-TA treated and CB cast BHJ active layers,

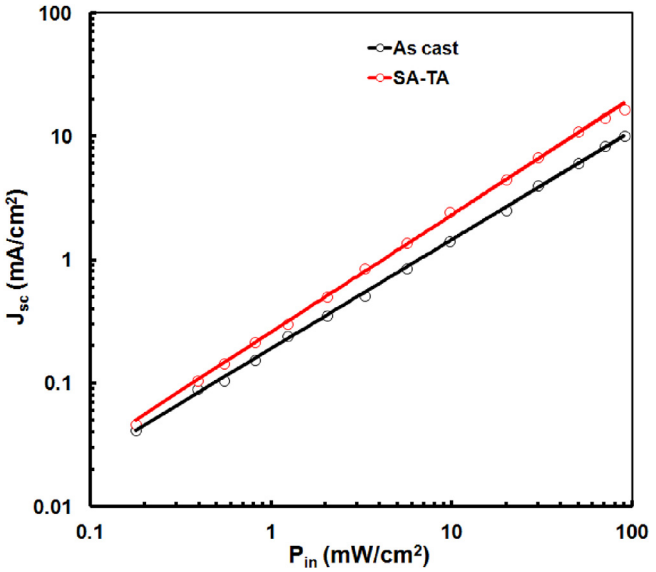

Fig. 7. Variation of Jsc with illumination intensity for the PSCs based on as cast and SA-TA treated active layers.

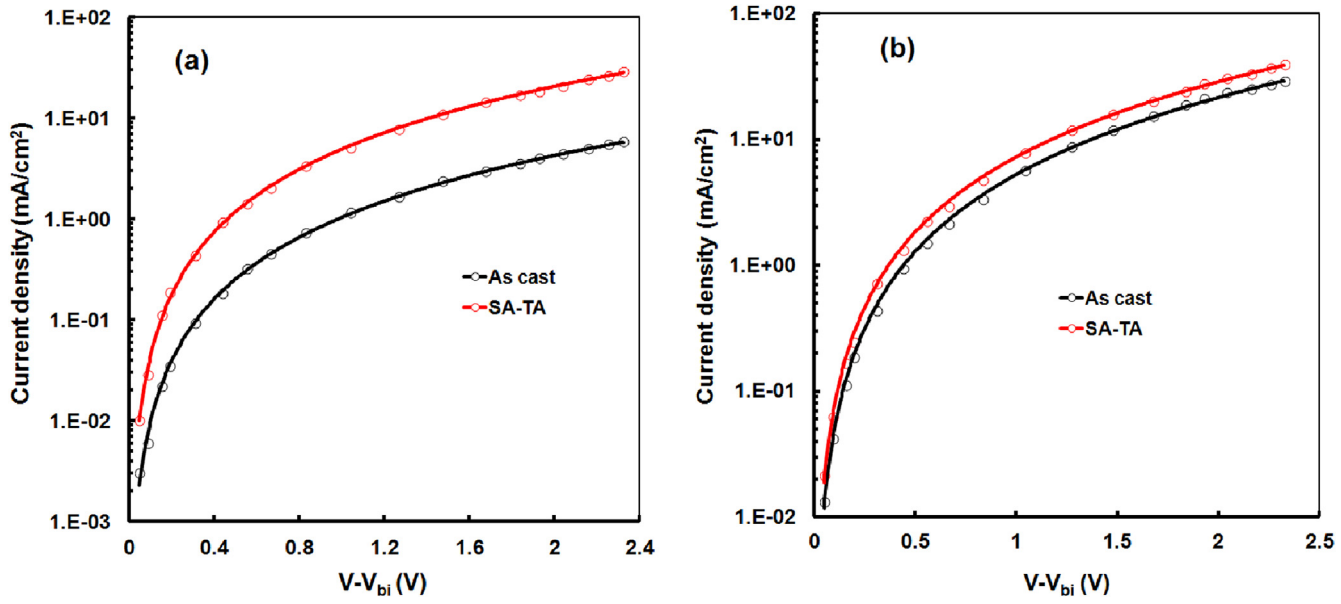

Fig. 6. J–V characteristic of the (a) hole- and (b) electron-device based on the as cast and SA-TA treated active layers.

respectively. This indicates that bimolecular recombination in the SA-TA treated PSC was significantly suppressed as compared to CB cast counterpart, which is consistent with the more balanced charge transport and increased value of FF.

The series resistance (R_s) and shunt resistance (R_{sh}) were estimated from the reciprocal of the slope of the J-V characteristics under illumination around J_{sc} and V_{oc}, respectively and are complied in the table. The decrease in the R_s from 17.45 to 8.6 Ω cm^2 and increase in R_{sh} from 418 to 624 Ω cm^2 in the CB cast and SA-TA processed based devices, respectively indicates efficient charge transport in vacuum dried BHJ film due to decrease in the trap-assisted Shockley −Read −Hall (SRH) recombination. Fig. 8 shows the dependence of V_{oc} with incident illumination intensity (P_{in}). The slope of the V_{oc} versus ln (P_{in}) is related to the degree of trap-assist or SRH recombination in BHJ PSCs [68,69]. It has been reported that in the case of trap-assisted recombination, V_{oc} strongly depends on the illumination intensity with the slope close to 2kT/q, where k is the Boltzmann's constant, T is absolute temperature and q is the electronic charge [70,71]. The PSC based on CB cast active layer shows a slope of 1.56 kT/q indicating strong SRH recombination whereas the SA-TA processed PSC exhibits a smaller slope of 1.37 kT/q. The lower value can be attributed to the improved charge transport due to the favorable active layer morphology and phase separation and increase in hole mobility induced by the SA-TA treatment.

The charge generation and exciton dissociation processes in the BHJ active layer of PSCs were investigated by performing the variation of photocurrent density (J_{ph}) with effective voltage (V_{eff}) for the device [72] and shown in Fig. 9. The J_{ph} is given by $J_{ph} = J_L$-J_D, where J_L and J_D are the current density under illumination and in dark, respectively. In the case of as cast device, J_{ph} shows very strong field dependence across a large range of V_{eff} and not fully saturates even at a high V_{eff} although reaches its saturation value of 13.53 mA/cm^2. The relatively low values of charge carrier mobilities for the as cast active layer means that a stronger internal electric field is needed to sweep out all of the charge carriers before they recombined which may be responsible for reduced J_{sc} in comparing to J_{phsat}. The exciton dissociation efficiency ($P_{diss} = J_{sc}/J_{phsat}$) was estimated for both the devices based on as cast and SA-TA processed active layers. The higher value of P_{diss} for PSC based on SA-TA (0.91) than that of as cast counterpart (0.86) may be a major contributor for high J_{sc} and FF.

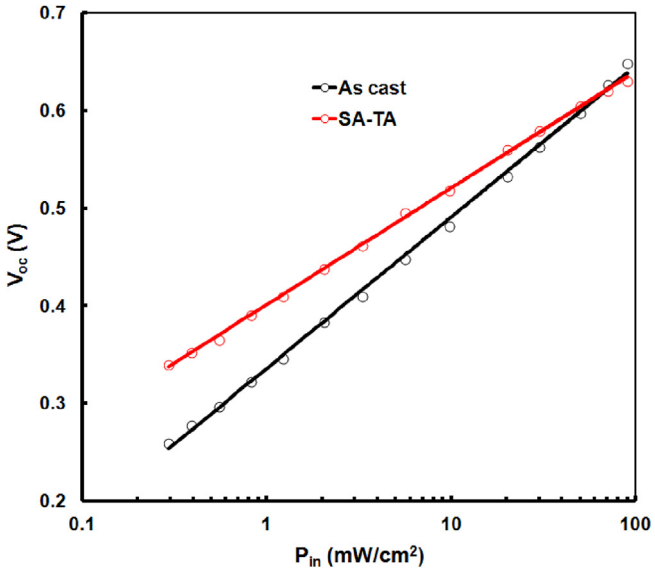

Fig. 8. Variation in open circuit voltage (V_{oc}) with incident light intensity (P_{in}) for PSCs based on as cast and SA-TA treated active layers.

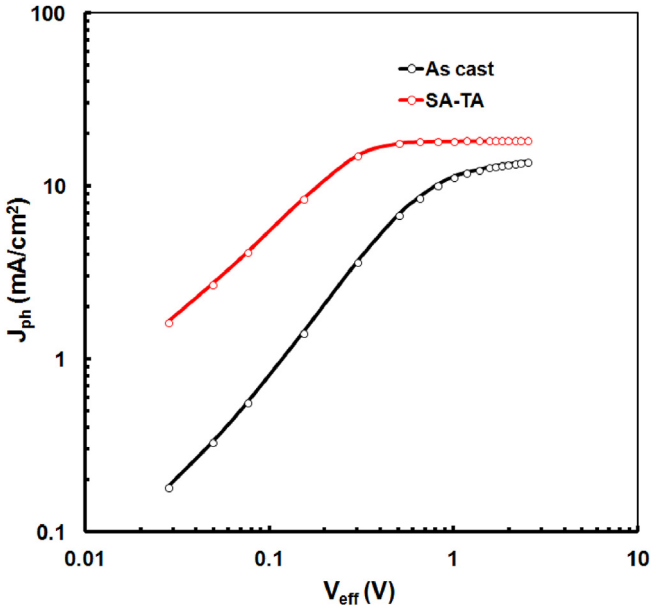

Fig. 9. Variation of photocurrent density (J_{ph}) with effective voltage (V_{eff}) for the PSCs based on as cast and SA-TA treated active layers.

The morphology of the as cast and SA-TA treated active layers are investigated by atomic force microscopy and shown in Fig. 10. The as cast film showed a smooth morphology with root mean square (RMS) value of 0.78 nm and poor phase separation between the donor and acceptor domains. This poor phase separation between the donor and acceptor hindered the charge transportation in the active layer leading to low FF and resulting low poor overall PCE. However, after SA-TA treatment the blend film showed relatively clearer phase separation and RMS value was also increased to 1.72 nm. The improved phase separation is in favor of forming bi-continuous interpenetrating networks for charge transport and reducing the bimolecular recombination, leads to high J_{sc} and FF for the PSC based on SA-TA active layer.

The XRD profile of the as cast and SA-TA treated **P**:$PC_{71}BM$ film is shown in Fig. 11. The as cast **P**:$PC_{71}BM$ film cast from the showed a broad (100) diffraction peak at $2\theta = 4.96°$, corresponds to the lamellar distance of 1.84 nm and also showed a wider band centered at $2\theta = 22.38°$, corresponds to the π-π stacking distance of 0.45 nm. The peak at $2\theta = 18.12°$ is corresponds to the PC71BM in the blend film. For the SA-TA treated film, the intensity of diffraction peaks were increased significantly, indicating more ordered π-π stacking and crystallinity of terpolymer induced by the SA- TA treatment, leading to the improved Jsc and FF.

We have determined the energy loss (E_{loss}) using the expression, $E_{loss} = E_g$-qV_{oc}, where, E_g is the lowest optical bandgap of the donor and acceptor, for the devices with optimized active layers based on **P** terpolymer and is 0.47 eV. The E_{loss} for the **P**:$PC_{71}BM$ active layer is lower than the threshold value of 0.6 eV. In our case, the LUMO offset (ΔE_{LL}) between **P** and $PC_{71}BM$ (LUMO = −4.10 eV) [35,55] is about 0.23 eV, which is lower than that threshold valve of 0.3 eV, for efficient exciton dissociation. Recently, Janssen et al. [73] and other researchers [74] have reported that PSCs for which E_{loss}<0.6 eV and ΔE_{LL} ~ 0.2 eV. Recently, PSC based on a D-A copolymer as donor showed overall PCE of about ~9.0% with ΔE_{LL} ~ 0.1 eV [70].

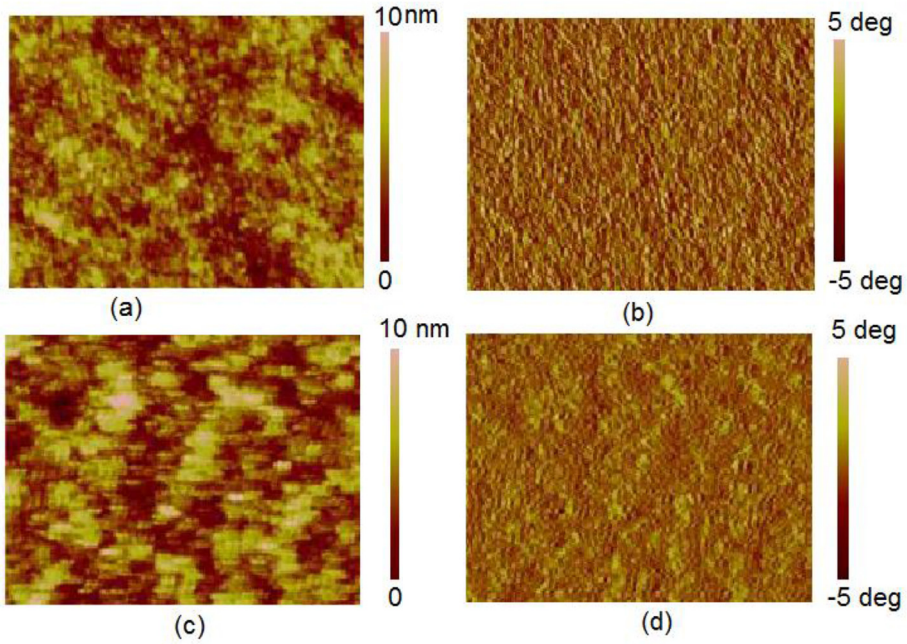

Fig. 10. AFM height images and AFM phase images, (a, b) the as cast film and (c, d) SA-TA treated film.

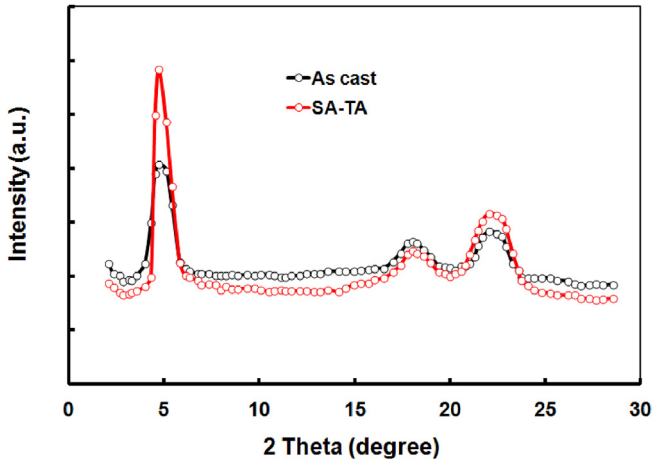

Fig. 11. X-ray diffraction patterns of as cast and SA-TA treated **P**:$PC_{71}BM$ thin films.

4. Conclusion

In summary, a low bandgap terpolymer **P** containing thiadiazoloquinoxaline and benzothiadiazole acceptors and thiophene as donor in its backbone was synthesized and investigated its optical and electrochemical properties. The **P** exhibits low optical bandgap of 1.12 eV and HOMO/LUMO energy levels of −5.25 eV/−3.87 eV, indicating that the efficient exciton dissociation is favorable in **P**:$PC_{71}BM$ BHJ active layer. After the optimization of **P** to $PC_{71}BM$ weight ratio, the BHJ PSC showed a moderate PCE of 4.10% and is further improved up to 7.24% with J_{sc} of 16.12 mA/cm^2, V_{oc} of 0.65 V and FF of 0.72. The increase in the PCE is related with the enhancement in the both J_{sc} and FF, attributed optimized nanoscale morphology of the active layer for both efficient exciton dissociation and charge transport towards the electrodes and balanced charge transport in the device, induced by the SA-TA treatment of active layer. To our best of our knowledge, PCE of 7.54% is also the highest for the PSCs with low bandgap of below 1.12 eV with low energy loss of 0.47 eV, which indicates that this terpolymer could be excellent candidate for the PSC employing ternary active layer and tandem device.

Acknowledgement

M.L. Keshtov, S.A. Kuklin, D.Y. Godovskiy, and N.A. Radychev thank the Russian Science Foundation (project no. 14–13–01444) for financial support.

Appendix A. Supplementary data

Supplementary data related to this article can be found at http://dx.doi.org/10.1016/j.orgel.2017.04.015.

References

[1] G.J. Hedley, A.J. Ward, A. Alekseev, C.T. Howells, E.R. Martins, L.A. Serrano, G. Cooke, A. Ruseckas, I.D.W. Samuel, Determining the optimum morphology in high-performance polymer-fullerene organic photovoltaic cells, Nat. Commun. 4 (2013) 2867.
[2] Y. Gu, C. Wang, T.P. Russell, Multi-length-scale morphologies in PCPDTBT/PCBM bulk-heterojunction solar cells, Adv. Energy Mater. 2 (2012) 683–690.
[3] L. Lu, T. Zheng, Q. Wu, A.M. Schneider, D. Zhao, L. Yu, Recent advances in bulk heterojunction polymer solar cells, Chem. Rev. 115 (2015) 12666–12731.
[4] L. Dou, Y. Liu, Z. Hong, G. Li, Y. Yang, Low-bandgap near-IR conjugated polymers/molecules for organic electronics, Chem. Rev. 115 (2015) 12633–12665.
[5] I.F. Domínguez, A. Distler, L. Lüer, Stability of organic solar cells: the influence of nanostructured carbon materials, Adv. Energy Mater. (2016) 1601320, http://dx.doi.org/10.1002/aenm.201601320.
[6] H. Yao, L. Ye, H. Zhang, S. Li, S. Zhang, J. Hou, Molecular design of benzodithiophene- based organic photovoltaic materials, Chem. Rev. 116 (2016) 7397–7457.
[7] G.J. Hadley, A. Ruseckas, I.D.W. Sumuel, Light harvesting for organic photovoltaics, Chem. Rev. 117 (2017) 796–837.
[8] J. Chen, J. Cao, Development of novel conjugated donor polymers for high-efficiency bulk-heterojunction photovoltaic devices, Acc. Chem. Res. 42 (2009) 171809–171810.
[9] J. Peet, A.J. Heeger, G.C. Bazan, "Plastic" solar cells: self-assembly of bulk heterojunction nanomaterials by spontaneous phase separation, Acc. Chem. Res. 42 (2009) 1700–1708.
[10] J.J.M. Halls, C.A. Walsh, N.C. Greenham, E.A. Marseglia, R.H. Friend, S.C. Moratti, A.B. Holmes, Efficient photodiodes from interpenetrating polymer networks, Nature 376 (1995) 498–500.

[11] G. Yu, J. Gao, J.C. Hummelen, F. Wudl, A.J. Heeger, Polymer photovoltaic cells - enhanced efficiencies via a network of internal donor-acceptor heterojunctions, Science 270 (1995) 1789–1791.

[12] J. You, L. Dou, K. Yoshimura, T. Kato, K. Ohya, T. Moriarty, K. Emery, C.C. Chen, J. Gao, G. Li, Y. Yang, A polymer tandem solar cell with 10.6% power conversion efficiency, Nat. Commun. 4 (2013) 1446.

[13] W. Li, K.H. Hendriks, W.S.C. Roelofs, Y. Kim, M.M. Wienk, R.A.J. Janssen, Efficient small bandgap polymer solar cells with high fill factors for 300 nm thick films, Adv. Mater. 25 (2013) 3182–3186.

[14] (a) H. Bin, L. Gao, Z.G. Zhang, Y. Yang, Y. Zhang, C. Zhang, S. Chen, L. Xue, C. Yang, M. Xiao, Y. Li, 11.4% efficiency non-fullerene polymer solar cells with trialkylsilyl substituted 2D conjugated polymer as donor, Nat. Commun. 24 (2016) 13651;
(b) Y. Lin, F. Zhao, Q. He, L. Huo, Y. Wu, T.C. Parker, W. Ma, Y. Sun, C. Wang, D. Zhu, A.J. Heeger, S.R. Marder, X. Zhan, High performance electron acceptor with thienyl side chains for organic solar cells, J. Am. Chem. Soc. 138 (2016) 15011–15018;
(c) J. Min, Z.G. Zhang, S. Zhang, Y. Li, Conjugated side chains isolated D-A copolymers based on benzo [1,2-b:4.5-b`]dithiophene –alt-dithienylbenzotriazole: synthesis and photovoltaic properties, Chem. Mater. 24 (2012) 3247–3254.

[15] N. Li, C. Brabec, Air-processed polymer tandem solar cells with power conversion efficiency exceeding 10%, Energy Environ. Sci. 8 (2015) 2902–2909.

[16] S.B. Dkhil, M. Pfannmöller, S. Bals, T. Koganezawa, N. Yoshimoto, D. Hannani, M. Gaceur, C. Videlot-Ackermann, O. Margeat, J. Ackermann, Square-centimeter- sized high-efficiency polymer solar cells: how the processing atmosphere and film quality influence performance at large scale, Adv. Energy Mater. 6 (2016) 1600290.

[17] L. Zuo, S. Zhang, H. Li, H. Chen, Toward highly efficient large-area ITO-free organic solar cells with a conductance-gradient transparent electrode, Adv. Mater. 27 (2015) 6983–6989.

[18] S. Hong, H. Kang, G. Kim, S. Lee, S. Kim, J.G., J.H. Lee, J. Lee, M. Yi, J. Kim, H. Back, J.R. Kim, K. Lee, A series connection architecture for large-area organic photovoltaic modules with a 7.5% module efficiency, Nat. Commun. 7 (2016) 10279.

[19] W. Zhao, D. Qian, S. Zhang, S. Li, O. Inganas, F. Gao, J. Hou, Fullerene-free polymer solar cells with over 11% efficiency and excellent thermal stability, Adv. Mater. 28 (2016) 4734–4739.

[20] J.W. Jung, J.W. Jo, W.H. Jo, Enhanced performance and air stability of polymer solar cells by formation of a self-assembled buffer layer from fullerene-end-capped poly(ethylene glycol), Adv. Mater. 23 (2011) 1782–1787.

[21] Y.F. Li, Molecular design of photovoltaic materials for polymer solar cells: toward suitable electronic energy levels and broad absorption, Acc. Chem. Res. 45 (2012) 723–733.

[22] C.J. Brabec, S. Gowrisanker, J.J.M. Halls, D. Laird, S. Jia, S.P. Williams, Polymer–fullerene bulk-heterojunction solar cells, Adv. Mater. 22 (2010) 3839–3856.

[23] J.W. Jung, F. Liu, T.P. Russell, W.H. Jo, A high mobility conjugated polymer based on dithienothiophene and diketopyrrolopyrrole for organic photovoltaics, Energy Environ. Sci. 5 (2012) 6857–6861.

[24] J.H. Kim, C.E. Song, N. Shin, H. Kang, S. Wood, I.N. Kang, B.J. Kim, B. Kim, J.S. Kim, W.S. Shin, D.H. Hwang, High-crystalline medium-band-gap polymers consisting of benzodithiophene and benzotriazole derivatives for organic photovoltaic cells, ACS Appl. Mater. Interfaces 5 (2013) 12820–12831.

[25] J.H. Kim, J.B. Park, D. Xu, D. Kim, J. Kwak, A.C. Grimsdale, D.H. Hwang, Effect of π-conjugated bridges of TPD-based medium bandgap conjugated copolymers for efficient tandem organic photovoltaic cells, Energy Environ. Sci. 7 (2014) 4118–4131.

[26] J. Zhao, Y. Li, G. Yang, K. Jiang, H. Lin, H. Ade, W. Ma, H. Yan, Efficient organic solar cells processed from hydrocarbon solvents, Nat. Energy 1 (2016) 15027.

[27] M.C. Scharber, D. Mühlbacher, M. Koppe, P. Denk, C. Waldauf, A.J. Heeger, C.J. Brabec, Design rules for donors in bulk-heterojunction solar cells—towards 10% energy-conversion efficiency, Adv. Mater. 18 (2006) 789–794.

[28] P.M. Beaujuge, C.M. Amb, J.R. Reynolds, Spectral engineering in π-conjugated polymers with intramolecular Donor–Acceptor interactions, Acc. Chem. Res. 43 (2010) 1396–1407.

[29] J. Roncali, Molecular engineering of the band gap of π-conjugated systems: facing technological applications, Macromol. Rapid Commun. 28 (2007) 1761–1775.

[30] K.H. Hendricks, G.H.J. Heintges, V.S. Gevaerts, M.M. Wienk, R.A.J. Janssen, High-molecular-weight regular alternating diketopyrrolopyrrole-based terpolymers for efficient organic solar cells, Angew. Chem. Int. Ed. 52 (2013) 8341–8344.

[31] Y.H. Chao, J.F. Jheng, J.S. Wu, K.Y. Wu, H.H. Peng, M.C. Tsai, C.L. Wang, Y.N. Hsiao, C.L. Wang, C.Y. Lin, C.S. Hsu, Porphyrin-incorporated 2D d–a polymers with over 8.5% polymer solar cell efficiency, Adv. Mater. 26 (2014) 5205–5210.

[32] M. Qian, R. Zhang, J. Hao, W. Zhang, Q. Zhang, J. Wang, Y. Tao, S. Chen, J. Fang, W. Huang, Dramatic enhancement of power conversion efficiency in polymer solar cells by conjugating very low ratio of triplet iridium complexes to PTB7, Adv. Mater. 27 (2015) 3546–3552.

[33] A. Kim, D.H. Lee, H.A. Um, J. Shin, M.J. Cho, D.H. Choi, Tunable light harvesting properties of a highly crystalline alternating terpolymer for high performing solar cells, Polym. Chem. 6 (2015) 5478–5486.

[34] S.B. Kim, H.A. Um, H.J. Kim, M.J. Cho, D.H. Choi, A diketopyrrolopyrrole-based regular terpolymer bearing two different π-extended donor units and its application in solar cells, Org. Electron. 31 (2016) 198–206.

[35] E.Y. Ko, G.E. Park, D.H. Lee, H.A. Um, J. Shin, M.J. Cho, D.H. Choi, Enhanced performance of polymer solar cells comprising diketopyrrolopyrrole-based regular terpolymer bearing two different π-extended donor units, ACS Appl. Mater. Interfaces 7 (2015) 28303–28310.

[36] H.J. Kim, G.E. Park, D.H. Lee, M.J. Cho, D.H. Choi, Importance of varying electron-accepting moieties in regular conjugated terpolymers for use in polymer solar cells, Org. Electron. 38 (2016) 256–263.

[37] T. Qin, W. Zajaczkowski, W. Pisula, M. Baumgarten, M. Chen, M. Gao, G. Wilson, C.D. Easton, K. Mullen, S.E. Watkins, Tailored donor–acceptor polymers with an A–D1–A–D2 structure: controlling intermolecular interactions to enable enhanced polymer photovoltaic devices, J. Am. Chem. Soc. 136 (2014) 6049–6055.

[38] M. Wang, H. Wang, T. Yokoyama, X. Liu, Y. Huang, Y. Zhang, T.Q. Nguyen, S. Aramaki, G.C. Bazan, High open circuit voltage in regioregular narrow band gap polymer solar cells, J. Am. Chem. Soc. 136 (2014) 12576–12579.

[39] Q. Tao, Y. Xia, X. Xu, S. Hedström, O. Bäcke, D.I. James, P. Persson, E. Olsson, O. Inganäs, L. Hou, W. Zhu, E. Wang, D–A1–D–A2 copolymers with extended donor segments for efficient polymer solar cells, Macromolecules 48 (2015) 1009–1016.

[40] T. Ma, K. Jiang, S. Chen, H. Hu, H. Lin, Z. Li, J. Zhao, Y. Liu, Y.M. Chang, C.C. Hsiao, H. Yan, A novel D-A1-D-A2 -type polymer that exhibits a small bandgap of 1.43 eV, Adv. Energy Mater. 5 (2015) 1501282.

[41] (a) N.A. Ran, J.A. Love, C.J. Takacs, A. Sadhanala, J.K. Beavers, S.D. Collins, Y. Huang, R.H. Friend, G.C. Bazan, T.Q. Nguyen, Harvesting the full potential of photons with organic solar cells, Adv. Mater. 28 (2016) 1482–1488;
(b) R.A.J. Janssen, J. Nelson, Factors limiting device efficiency in organic photovoltaic devices, Adv. Mater. 25 (2013) 1847–1858.

[42] H. Lv, X. Zhao, Z. Li, D. Yang, Z. Wang, X. Yang, Fluorinated low bandgap copolymer based on dithienosilole–benzothiadiazole for high-performance photovoltaic device, Polym. Chem. 5 (2014) 6279–6286.

[43] A.C. Stuart, J.R. Tumbleston, H. Zhou, W. Li, S. Liu, H. Ade, W. You, Fluorine substituents reduce charge recombination and drive structure and morphology development in polymer solar cells, J. Am. Chem. Soc. 135 (2013) 1806–1815.

[44] J.W. Jo, S. Bae, F. Liu, T.P. Russell, W.H. Jo, Comparison of two D–A type polymers with each being Fluorinated on D and a unit for high performance solar cells, Adv. Funct. Mater. 25 (2014) 120–125.

[45] W. Li, S. Albrecht, L. Yang, S. Roland, J.R. Tumbleston, T. McAfee, L. Yan, M.A. Kelly, H. Ade, D. Neher, W. You, Mobility-controlled performance of thick solar cells based on fluorinated copolymers, J. Am. Chem. Soc. 136 (2014) 15566–15576.

[46] H.J. Son, W. Wang, T. Xu, Y. Liang, Y. Wu, G. Li, L. Yu, Synthesis of fluorinated polythienothiophene-co-benzodithiophenes and effect of fluorination on the photovoltaic properties, J. Am. Chem. Soc. 133 (2011) 1885–1894.

[47] Y. Liu, J. Zhao, Z. Li, C. Mu, W. Ma, H. Hu, K. Jiang, H. Lin, H. Ade, H. Yan, Aggregation and morphology control enables multiple cases of high-efficiency polymer solar cells, Nat. Commun. 5 (2014) 5293–5301.

[48] H. Hu, K. Jiang, G. Yang, J. Liu, Z. Li, H. Lin, Y. Liu, J. Zhao, J. Zhang, F. Huang, Y. Qu, W. Ma, H. Yan, Terthiophene-based D–A polymer with an asymmetric arrangement of alkyl chains that enables efficient polymer solar cells, J. Am. Chem. Soc. 137 (2015) 14149–14157.

[49] J.D. Chen, C. Cui, Y.Q. Li, L. Zhou, Q.D. Ou, C. Li, Y. Li, J.X. Tang, Single-junction polymer solar cells exceeding 10% power conversion efficiency, Adv. Mater. 27 (2015) 1035–1041.

[50] H. Zhong, C.Z. Li, J. Carpenter, H. Ade, A.K.J. Jen, Influence of regio- and chemoselectivity on the properties of fluoro-substituted thienothiophene and benzodithiophene copolymers, J. Am. Chem. Soc. 137 (2015) 7616–7619.

[51] X. Liu, B.B.Y. Hsu, Y. Sun, C.K. Mai, A.J. Heeger, G.C. Bazan, High thermal stability solution-processable narrow-band gap molecular semiconductors, J. Am. Chem. Soc. 136 (2014) 16144–16147.

[52] Y. Ji, C. Xiao, Q. Wang, J. Zhang, C. Li, Y. Wu, Z. Wei, X. Zhan, W. Hu, Z. Wang, R.A.J. Janssen, W. Li, Asymmetric diketopyrrolopyrrole conjugated polymers for field-effect transistors and polymer solar cells processed from a non-chlorinated solvent, Adv. Mater. 28 (2016) 943–950.

[53] M.L. Keshtov, I.O. Konstantinov, M.M. Krayushkin, S.A. Kuklin, S.M. Masoud, S.N. Osipov, A.R. Khokhlov, New electron accepting quinoxalinothiadiazole containing heterocycles as promising building blocks for organic optoelectronic devices, Dokl. Chem. 468 (2) (2016) 202–207.

[54] R.B. Zerdan, P. Cohn, E. Puodziukynaite, M.B. Baker, M. Voisin, C. Sarun, R.K. Castellano, Synthesis, optical properties and electronic structures of nucleobase-containing π-conjugated oligomers, J. Org. Chem. 80 (2015) 1828.

[55] Q. Yin, J.S. Miao, Z. Wu, Z.F. Chang, J.L. Wang, H.B. Wu, Y. Cao, Rational design of diketopyrrolopyrrole-based oligomers for high performance small molecular photovoltaic materials via an extended framework and multiple fluorine substitution, J. Mater. Chem. A 3 (2015) 11575–11586.

[56] M. L. Keshtov, S. A. Kuklin, N. A. Radychev, I. E. Ostapov, A.Y. Nikolaev I.O. Konstantinov, M. M. Krayushkin, E.N. Koukarasd, Abhishek Sharma, G. D. Sharma, Synthesis of new D-A1-D-A2 type low bandgap terpolymers based on different thiadiazoloquinoxaline acceptor units for efficient polymer solar cells, RSC Adv. http://dx.doi.org/10.1039/C6RA14537J.

[57] J.P. Perdew, K. Burke, M. Ernzerhof, Generalized Gradient approximation made simple, Phys. Rev. Lett. 77 (1996) 3865–3868.

[58] (a) A.D. Becke, Density functional thermochemistry III the role of exact

exchange, J. Chem. Phys. 98 (1993) 5648–5652;
(b) C. Lee, W. Yang, R.G. Parr, Development of the Colle-Salvetti correlation-energy formula into a functional of the electron density, Phys. Rev. B 37 (1988) 785–789.
[59] Y. Zhao, D.G. Truhlar, The M06 suite of density functionals for main group thermochemistry, thermochemical kinetics, noncovalent interactions, excited states, and transition elements: two new functionals and systematic testing of four M06-class functionals and 12 other functionals, Theor. Chem. Acc. 120 (2008) 215–241.
[60] D. Deng, Y. Zhang, J. Zhang, Z. Wang, L. Zhu, J. Fang, B. Xia, Z. Wang, K. Lu, W. Ma, Z. Wei, Fluorination-enabled optimal morphology leads to over 11% efficiency for inverted small-molecule organic solar cells, Nat. Comm. 7 (2016) 13740.
[61] I. Etxebarria, J. Ajuria, R. Pacios, Solution-processable polymeric solar cells: a review on materials, strategies and cell architectures to overcome 10%, Org. Electron. 19 (2015) 34–60.
[62] S. Kwon, H. Kang, J.H. Lee, J. Lee, S. Hong, H. Kim, K. Lee, Effect of processing additives on organic photovoltaics: recent progress and future prospects, Adv. Energy Mater. (2016) 1601496.
[63] A. Bagui, S.S.K. Iyer, Effect of solvent annealing in the presence of electric field on P3HT: PCBM films used in organic solar cells, IEEE Trans. Electron Devices 58 (2011) 4061–4066.
[64] V. Suman, A. Gupta, S.P. Bagui, Singh, molecular engineering of highly efficient small molecule nonfullerene acceptor for organic solar cells, Adv. Funct. Mater. (2016), http://dx.doi.org/10.1002/adfm.201603820.
[65] C.M. Proctor, C. Kim, D. Neher, T.Q. Nguyen, Nongeminate recombination and charge transport limitations in diketopyrrolopyrrole-based solution-processed small molecule solar cells, Adv. Funct. Mater. 23 (2013) 3584–3594.
[66] J.W. Jung, J.W. Jo, C.C. Chueh, F. Liu, W.H. Jo, T.P. Russell, A.K.Y. Jen, Fluoro-Substituted n-type conjugated polymers for additive-free all-polymer bulk heterojunction solar cells with high power conversion efficiency of 6.71%, Adv. Mater. 27 (2015) 3310–3317.
[67] O.K. Kwon, J.H. Park, D.W. Kim, S.K. Park, S.Y. Park, An all-small-molecule organic solar cell with high efficiency non-fullerene acceptor, Adv. Mater. 27 (2015) 1951–1956.
[68] S.R. Cowan, A. Roy, A.J. Heeger, Recombination in polymer-fullerene bulk heterojunction solar cells, Phys. Rev. B 82 (2010) 245207.
[69] L.J.A. Koster, V.D. Mihailetchi, R. Ramaker, P.W.M. Blom, Light intensity dependence of open-circuit voltage of polymer : fullerene solar cells, Appl. Phys. Lett. 86 (2005) 123509.
[70] V. Gupta, A.K.K. Kyaw, D.H. Wang, S. Chand, G.C. Bazan, A.J. Heeger, Barium: an efficient cathode layer for bulk-heterojunction solar cells, Sci. Rep. 3 (2013) 1965.
[71] A.K.K. Kyaw, D.H. Wang, V. Gupta, W.L. Leong, L. Ke, G.C. Bazan, A.J. Heeger, Intensity dependence of current–voltage characteristics and recombination in high-efficiency solution-processed small-molecule solar cells, ACS Nano 7 (2013) 4569–4577.
[72] L. Wu, F.C. Chen, Y.S. Hsiao, F.C. Chien, P.L. Chen, C.H. Kuo, M.H. Huang, C.S. Hsu, Surface plasmonic effects of metallic nanoparticles on the performance of polymer bulk heterojunction solar cells, ACS Nano 5 (2011) 959–967.
[73] W.W. Li, K.H. Hendriks, A. Furlan, M.M. Wienk, R.A.J. Janssen, High quantum efficiencies in polymer solar cells at energy losses below 0.6 eV, J. Am. Chem. Soc. 137 (2015) 2231.
[74] (a) K. Gao, L.S. Li, T.Q. Lai, L.G. Xiao, Y. Huang, F. Huang, J.B. Peng, Y. Cao, F. Liu, T.P. Russell, R.A.J. Janssen, X.B. Peng, Deep absorbing porphyrin small molecule for high-performance organic solar cells with very low energy losses, J. Am. Chem. Soc. 137 (2015) 7282;
(b) X.F. Liu, Y.M. Sun, B.B.Y. Hsu, A. Lorbach, L. Qi, A.J. Heeger, G.C. Bazan, Design and properties of intermediate-sized narrow band-gap conjugated molecules relevant to solution-processed organic solar cells, J. Am. Chem. Soc. 136 (2014) 5697–5708;
(c) Z.Y. Zhang, F. Lin, H.C. Chen, H.C. Wu, C.L. Chung, C. Lu, S.H. Liu, S.H. Tung, W.C. Chen, K.T. Wong, P.T. Chou, A silole copolymer containing a ladder-type heptacylic arene and naphthobisoxadiazole moieties for highly efficient polymer solar cells, Energy Environ. Sci. 8 (2015) 552–557;
(d) Q. Peng, Q. Huang, X.B. Hou, P.P. Chang, J. Xu, S.J. Deng, Enhanced solar cell performance by replacing benzodithiophene with naphthodithiophene in diketopyrrolopyrrole-based copolymers, Chem. Commun. 48 (2012) 11452–11454;
(e) J.W. Jung, F. Liu, T.P. Russell, W.H. Jo, A high mobility conjugated polymer based on dithienothiophene and diketopyrrolopyrrole for organic photovoltaics, Energy Environ. Sci. 5 (2012) 6857–6861;
(f) K. Kawashima, Y. Tamai, H. Ohkita, I. Osaka, K. Takimiya, High-efficiency polymer solar cells with small photon energy loss, Nat. Commun. 6 (2015) 10085.